mater.scichina.com link.springer.com

Published online 28 July 2022 | https://doi.org/10.1007/s40843-022-2108-4
Sci China Mater 2023, 66(1): 169–178

Solvent-free synthesis of Co@NC catalyst with Co–N species as active sites for chemoselective hydrogenation of nitro compounds

Haisheng Wei[1†], Huaxing Song[1†], Yujing Ren[3†], Xiaorui Yan[1], Geqian Fang[2], Wenhua Wang[1], Wanzhong Ren[1], Mingyuan Zhu[1] and Jian Lin[2*]

ABSTRACT **Metal-organic frameworks (MOFs) derived Co-based catalysts have received extensive attention in the chemoselective hydrogenation of nitroarenes, while they usually require a lot of solvent during the synthesis and identification of active species. This study explores a solid-phase synthesis strategy to obtain MOF precursors without using any solvent, which is then foamed and pyrolyzed to synthesize the Co@NC-X catalyst. It was found that a nitrogen-doped graphene shell can well encapsulate the Co nanoparticles. The resulting catalyst, which was pyrolyzed at 800°C, exhibited ~100% conversion for the hydrogenation of 3-nitrostyrene and >99% selectivity to 3-vinylaniline. This catalyst also showed excellent stability and good substrate universality for the hydrogenation of extensive substituted nitroarenes. Various characterizations revealed a positive relationship between the catalytic performance and the content of Co–N species tuned by pyrolysis temperature. This work provides a novel and green strategy to design an efficient Co-based catalyst for chemoselective hydrogenation.**

Keywords: solvent-free synthesis, Co-based catalyst, nitroarenes, selective hydrogenation, Co–N species

INTRODUCTION

Catalytic hydrogenation of nitroarenes containing reducible groups is considered as an important way to synthesize corresponding functional anilines [1–3], which have widespread applications in the field of fine chemicals, such as pharmaceuticals, dyes, spices, and pesticides [4,5]. Heterogeneous catalysts of supported metals have received much attention due to their low pollution, easy separation, and good recyclability [6–8]. The main challenge in such a reaction is to reduce the nitro group preferentially while keeping the other sensitive groups unchanged. Conventionally, precious metal (such as Pt, Pd, Ru, Ir, and Au)-based catalysts with elaborate designs have achieved good performance in the chemoselective hydrogenation of nitro compounds [9–16], but they are not cost effective [17,18]. It is, thus, of great significance to develop efficient non-noble metal catalysts in the field of chemoselective hydrogenation [19,20], such as Co, Fe, Ni, and Cu-based catalysts, due to their unique catalytic performance [21–27]. Co-based catalysts have attracted increasing attention, and the effects of various parameters, such as support properties, cobalt precursor, and posttreatment, on the hydrogenation performance have extensively been investigated [5,28,29].

Recently, the pyrolytic transformation of metal-organic frameworks (MOFs) has been considered as a facile route to synthesize nitrogen-doped porous carbon-supported Co-based catalysts [30–33]. ZIF-67 is a widely studied MOF precursor that can pyrolyze to generate active Co components under an inert atmosphere at different decomposition temperatures or after various posttreatments [30–32]. However, the state-of-the-art method necessitates the fabrication of crystalline ZIF-67 MOF precursors using a substantial amount of solvent (such as methanol, water, ethanol, and *N*,*N*-dimethylformamide (DMF)). Moreover, it requires a complex washing procedure to eliminate uncoordinated ligands [34–36]. This excess usage of solvents and insufficient recycling protocols can bring about severe environmental problems. Moreover, the relationship between the doped nitrogen species bonding on Co nanoparticles (NPs) and the hydrogenation performance needs further clarification, particularly based on the electronic effects of nitrogen species on the Co sites and the activation of reactants.

This work proposes a solvent-free strategy for synthesizing nitrogen-doped graphene shell encapsulated Co species catalyst. The precursors of ZIF-67 and ZIF-8, such as cobaltous nitrate, zinc nitrate, and 2-methylimidazole (2-MeIM), were mixed in a solid state without any solvent assistance, then foamed and pyrolyzed, where the pyrolysis temperature was modulated in detail. It was discovered that following pyrolysis at 800°C, the resulting catalyst (Co@NC-800) could achieve 100% conversion and >99% selectivity of 3-vinylaniline under relatively mild reaction conditions for the selective hydrogenation of 3-nitrostyrene. Moreover, this catalyst exhibited good cyclic stability and general applicability in the hydrogenation of various substituted nitro compounds. A series of characterizations demonstrated that the Co sites with a slightly positive state by bonding with N species could play as the active component with a positive relationship to the catalytic performance.

[1] College of Chemistry and Chemical Engineering, Yantai University, Yantai 264005, China
[2] CAS Key Laboratory of Science and Technology on Applied Catalysis, Dalian Institute of Chemical Physics, Chinese Academy of Sciences, Dalian 116023, China
[3] Interdisciplinary Research Center of Biology & Catalysis, School of Life Sciences, Northwestern Polytechnical University, Xi'an 710072, China
[†] These authors contributed equally to this work.
[*] Corresponding author (email: jianlin@dicp.ac.cn)

 © Science China Press and Springer-Verlag GmbH Germany, part of Springer Nature 2022

EXPERIMENTAL SECTION

Materials

Zinc nitrate hexahydrate ($Zn(NO_3)_2{\cdot}6H_2O$), cobalt nitrate hexahydrate ($Co(NO_3)_2{\cdot}6H_2O$), ethanol, and toluene were purchased from Sinopharm Chemical Reagent Co., Ltd. (China) with analytical grade. 2-MeIM (98%), 3-nitrostyrene (96%), and 1,3,5-trimethylbenzene (≥99%, standard internal substance) were purchased from Aladdin Chemical Co., Ltd. (Shanghai, China). Other reaction substrates were purchased from Macklin Biochemical Co., Ltd. (Shanghai, China). All reagents were used without further purification.

Synthesis process

First, 10 mmol zinc nitrate hexahydrate, 4.5 mmol cobalt nitrate hexahydrate, and 29 mmol 2-MeIM were mixed and stirred for 10 min to form a solid mixture that corresponded to the formulation of ZIF-8 or ZIF-67 precursor. Then, the foaming material was obtained by drying the mixture at 120°C for 24 h. Second, the foaming material was fully ground and pyrolyzed at different temperatures for 2 h under a nitrogen atmosphere at 5°C min^{-1}. The resultant materials were denoted as Co@NC-X, where X was the pyrolysis temperature. No solvent was used in the entire preparation process.

Characterization

The content of metallic Co was determined using an inductively coupled plasma optical emission spectrometer (ICP-OES, Agilent 5110). Specifically, the amount of metal Co in the Co-based catalysts was detected using microwave digestion with solid samples to obtain a clear solution. The leaching of metal Co in the solution was conducted by evaporating the filtration solution and dissolving the residue in aqua regia, and then further diluted to the appropriate concentration for measurement.

X-ray diffraction (XRD) patterns were obtained on a D/max 2550 with Cu Kα radiation (λ = 0.15406 nm). The measurement range of 2θ was controlled from 5° to 80° with a rate of 5° min^{-1}.

The scanning electron microscopy (SEM) images were observed using a JSM-7900F (JEOL, Japan) by spray-gold processing to make the samples conductive.

Transmission electron microscopy (TEM) images were obtained on a JEM-1400 Plus electron microscope with an acceleration voltage of 200 kV. The histograms of the particle size distribution of Co NPs in the catalysts were obtained after counting ~200 particles in the images. High-resolution TEM (HRTEM) images were obtained on an FEI TF20 microscope equipped with a Super-X energy dispersive spectroscopy (EDS) attachment. The information on lattice spacing was obtained by measuring HRTEM images with digital micrograph software.

The X-ray absorption fine structure (XAFS) analysis of Co K-edge was conducted at the Shanghai Synchrotron Radiation Facility (Shanghai, China) using a Si(111) crystal monochromator on the BL11B beamline. Before the test, samples were pressed into thin sheets of 1 cm in diameter and sealed with Kapton tape film. The XAFS spectra were collected at 25°C using a 4-channel silicon drift detector Bruker 5040. Co K-edge extended XAFS (EXAFS) spectra were collected in a transmission mode. There were negligible changes in the line shape and peak position of Co K-edge X-ray absorption near-edge structure (XANES) spectra between two scans taken for a specific sample. The XAFS spectra of these standard samples (Co foil and Co_2O_3) were recorded in a transmission mode. The spectra were processed and analyzed using the software codes Athena and Artemis.

X-ray photoelectron spectroscopy (XPS) measurements were performed on a Thermo Scientific K-Alpha equipped with a monochromatized Al Kα X-ray source (1486.6 eV) to get the surface properties of the sample. The adopted results were corrected using the C 1s orbital (284.8 eV).

The N_2 adsorption-desorption characterization was conducted on a Micromeritics ASAP 2460 at 77 K. The density functional theory method was used to obtain the pore size distribution data.

Fourier transform infrared spectroscopy (FT-IR) patterns were collected on a Shimadzu IR Affinity-1S from 400 to 4000 cm^{-1} to measure the transmittance of the samples. The samples were dried at 120°C for 1 h to remove moisture, then adequately mixed with KBr (sample:KBr = 1:200) and finally pressed into transparent sheets and placed in the instrument to measure the transmittance.

Catalytic performance test

The hydrogenation reaction of the aromatic nitro compound was conducted in a 15-mL stainless steel reactor with a polytetrafluoroethylene liner. Typically, a mixture of 0.05 g catalyst, 0.5 mmol nitroarene, 0.25 mmol 1,3,5-trimethylbenzene (internal standard), and 5 mL toluene was introduced into the reactor at room temperature. Next, the air in the reactor was replaced with hydrogen six times. Then, the autoclave was charged with H_2 until 3 MPa and heated to 80°C in a water bath with a magnetic stirrer to initiate the reaction. After the completion of the reaction, the catalyst was centrifuged, and then the reaction solution was analyzed on an Agilent 7890B gas chromatograph equipped with an HP-5 column and flame ionization detector. The information of each component in the product was determined using gas chromatography-mass spectrometer (GC-MS, Agilent 5977B) equipped with an HP-5 type chromatographic column. The catalyst was separated and directly applied to the next run in the cyclic test. Additionally, to determine whether the catalytic process was heterogeneous, a hot filtration experiment was performed when the reaction proceeded for 30 min, and the filtered solution continued to react.

RESULTS

Synthesis and characterizations of Co@NC-X catalysts

A new synthesis method proceeding in the solid-state for a Co-based catalyst is explored because of the environmentally benign process. As shown in Scheme 1, the mixture of zinc nitrate hexahydrate, cobalt nitrate hexahydrate, and 2-MeIM is adequately stirred for 10 min without adding any solvent. In this process, the Co^{2+} ion, Zn^{2+} ion, and 2-MeIM ligand form a purple solid Co-Zn mixture by the coordination reaction. With further polymerization by drying at 120°C, the solid mixture melts into a brown state, then starts to swell and forms a nigger-brown material with a foaming pattern. Finally, the foamed composites are pyrolyzed under an inert atmosphere to obtain Co-based materials, denoted as Co@NC-X catalysts, where X represents the pyrolysis temperature.

The evolvement process of the target catalyst was further tracked using XRD, FT-IR, and SEM characterizations. As shown in Fig. 1a, the Co-Zn mixture shows complicated diffraction peaks compared with the corresponding precursors,

 © Science China Press and Springer-Verlag GmbH Germany, part of Springer Nature 2022

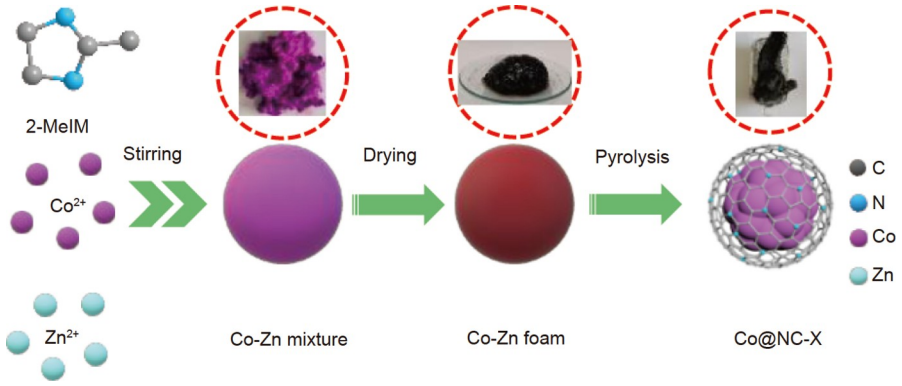

Scheme 1 Schematic illustration of the preparation process of Co@NC-X.

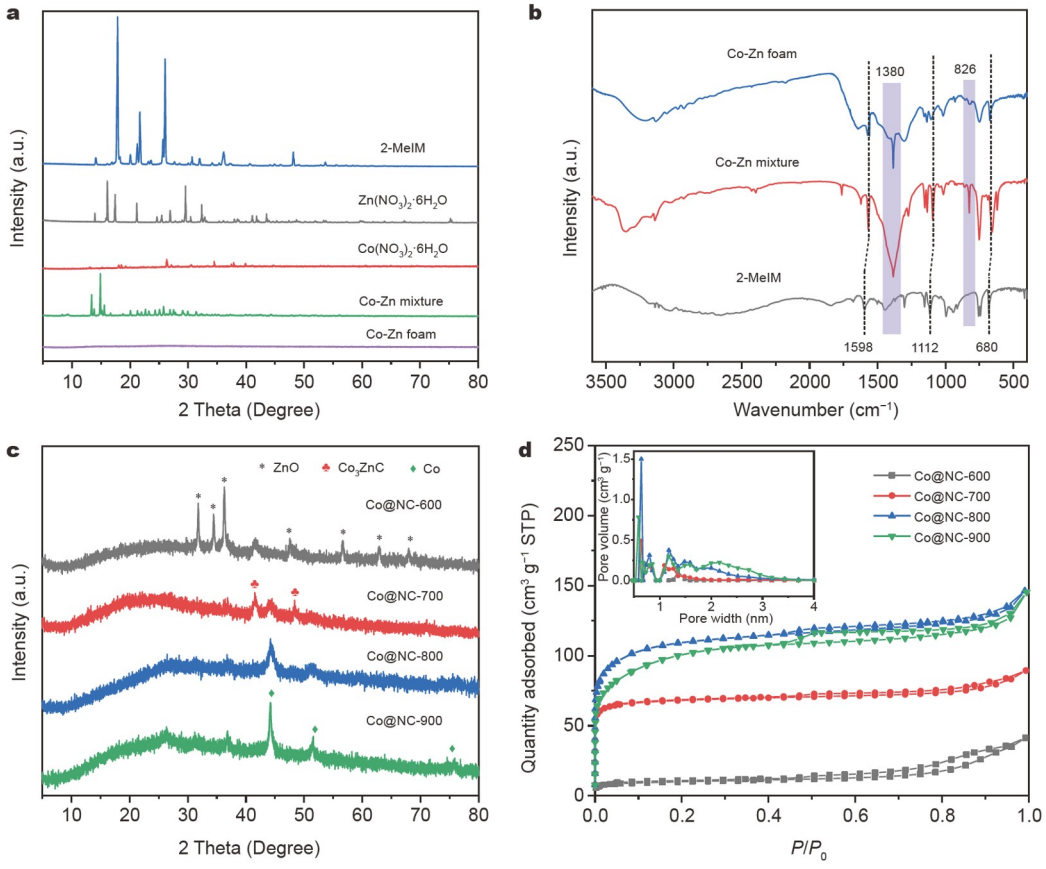

Figure 1 (a) XRD patterns of the precursor, Co-Zn mixture, and foaming material, (b) FT-IR analysis of the Co-Zn mixture and foaming material (the dashed lines show the shift of absorption peaks and the purple shadows show the production of new absorption peaks), (c) XRD patterns, and (d) N_2 adsorption-desorption isotherms of Co@NC-X catalysts with different pyrolysis temperatures (the inset shows the distribution of the corresponding pore size).

which may be attributed to the formation of the Zn_xCo_{1-x}-$(C_4H_6N_2)$ MOF structure [37]. After the drying treatment, the crystalline structure disappears. The corresponding FT-IR results in Fig. 1b indicate that the materials acquired after blending and drying procedures exhibit an obvious shift of peaks (such as from 1598, 1112, and 680 to 1571, 1092, and 665 cm^{-1}, respectively) along with the production of new absorption peaks (such as 1380 and 826 cm^{-1}) compared with the 2-MeIM ligand, which can be due to the coordination between the metal and ligand. Additionally, the morphology of the obtained materials is altered correspondingly, which transforms from a sheet structure into a compact structure after the drying treatment (Fig. S1). Therefore, combined with the above analysis, it is revealed that the components of Zn^{2+}, Co^{2+}, and 2-MeIM ligand engender strong interaction at an earlier stage but with low surface area (Table S1).

Further pyrolysis treatment is required to obtain the desired material, and the influence of pyrolysis temperature on the foaming material is investigated in detail. In the pyrolysis process, the 2-MeIM ligand decomposes and transforms into N-doped carbon, coupled with the reduction of the Co^{2+} ions and Zn evaporation. As shown in Fig. 1c, the material pyrolyzed at

 © Science China Press and Springer-Verlag GmbH Germany, part of Springer Nature 2022

600°C mainly displays the diffraction peaks attributed to ZnO and Co_3ZnC species (JCPDS No. 29-0524). When the calcination temperature increases from 600 to 900°C, the ZnO-related diffraction peaks become weaker and gradually disappear due to the Zn evaporation. Meanwhile, the intensity of the metallic Co-related diffraction peak increases, with values of 44.2°, 51.5°, and 75.9°, attributed to the (111), (200), and (220) planes of face-centered-cubic (fcc)-structured cobalt, respectively. The treatment at 800°C leads to the presence of metallic Co species-related diffraction peaks (JCPDS No. 15-0806). Moreover, the functional groups present in the foaming materials disappear on the pyrolyzed materials according to FT-IR spectra (Fig. S2), indicating the complete decomposition of the 2-MeIM ligand. Additionally, the morphology of different pyrolyzed catalysts was determined using SEM characterizations. As shown in Fig. S3, the materials become more fragmented with increasing pyrolysis temperature, producing porous structures on the surface.

N_2 adsorption-desorption isotherm measurements further confirm the porosity of the Co@NC-X catalysts. As shown in Fig. 1d, with the increase in pyrolysis temperature, more microporous (<1 nm) and mesoporous structures (2–3 nm) appear. Meanwhile, the Brunauer-Emmett-Teller (BET) surface area rises from 32.8 $m^2 g^{-1}$ on Co@NC-600 to 334.5 $m^2 g^{-1}$ on Co@NC-800, while a higher pyrolyzed temperature of 900°C results in a slightly lower surface area of 318.8 $m^2 g^{-1}$ on Co@NC-900 (Table S1).

The particle size and configuration of the Co@NC-800 catalyst were then characterized using HRTEM and high-angle annular dark-field TEM (HAADF-STEM). As shown in Fig. 2a and b, the lattice distance of Co NPs is 0.20 nm, which is assigned to the (111) facet of the Co^0 crystal. The mean size of Co particles is 9.3 nm by statistical analysis of ~200 particles, as shown in Fig. S4c. Comparatively, the other Co@NC-X catalysts show a similar size distribution at 8.7–9.6 nm, agreeing with the XRD results (Table S1). Besides, a characteristic lattice spacing of 0.34 nm in the shell is observed on Co@NC-800, which belongs to the (002) crystal plane of graphitic carbon. Thus, the Co NPs are covered by a graphene shell with a thickness of 1.5–5 nm.

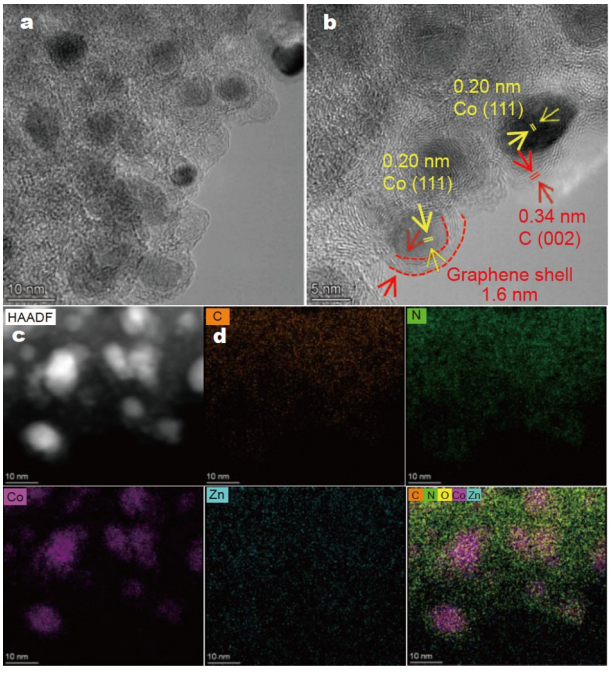

Figure 2 (a, b) HRTEM, (c) HAADF-STEM, and (d) EDS images of the Co@NC-800 catalyst. The red dashed line represents the graphene layer.

To identify the metallic Co NPs and the elemental composition in the Co@NC-800 sample, HAADF-STEM with EDS spectra was performed. As shown in Fig. 2c, the white granules observed by contrast degree represent the metallic Co NPs in the catalyst. The elemental mappings in Fig. 2d show that C, N, O, and Zn elements are uniformly dispersed in the catalyst. The overlapping image clearly shows that the Co particles are wrapped in the carbon layer doped with nitrogen species. This structure can be reflected using XPS analysis [38]. As shown in Fig. S5, there is a Co 2p signal in the Co@NC-800 catalyst, but with weak intensity. Moreover, the atomic ratio of surface Co/C is quite low, at only 0.021%. These results indicate that the N-doped graphene shell encapsulates the Co NPs.

Selective hydrogenation performance

To evaluate the catalytic performance of different Co@NC-X catalysts, the chemoselective hydrogenation of 3-nitrostyrene was selected as a probe reaction, which is the most demanding reaction in various substituted nitroarenes due to the more reactive C=C group toward hydrogenation than the nitro group in the molecule [39]. It can be seen that the Co@NC-600 catalyst exhibits poor activity and selectivity to the target product (Table 1, entry 1). As the pyrolysis temperature rises to 700°C, the performance obviously improves, obtaining 53.4% conversion and 98.5% selectivity within 4 h, similar to those on Co@NC-900 catalyst (Table 1, entries 2 and 4). In contrast, the Co@NC-800 catalyst exhibits the highest performance, achieving 100% conversion and >99% selectivity within 2 h (Table 1, entry 3). The turnover frequency (TOF) of different pyrolyzed catalysts is calculated based on the Co NPs' dispersion [40]. The results in Table 1 indicate that the Co@NC-800 catalyst possesses the highest TOF value among the Co@NC-X catalysts. Moreover, compared with previous reports on the chemoselective hydrogenation of 3-nitrostyrene [18,26,41–44], the Co@NC-800 catalyst exhibits much higher activity and selectivity while at rather milder conditions (Table S2).

The cyclic stability is an important parameter for evaluating the catalytic performance. The stability results on Co@NC-800 in Fig. S6a show that the activity and selectivity remain unchanged during five cycles. The catalyst after the cyclic run was further analyzed using XRD and XPS characterizations. As shown in Fig. S7, the intensity of the Co diffraction peak located at 44.2° is the same as the fresh catalyst, indicating that the Co species do not assemble during the reaction. Moreover, the ICP test confirmed no leaching of Co species following the reaction. The XPS analysis also demonstrates that the ratio of Co–N/C in the catalyst after the cyclic test is 0.025, which is similar to 0.024 in the fresh catalyst (Fig. S8 and Table S3). All these results confirm the high stability of the Co@NC-800 catalyst in the hydrogenation of 3-nitrostyrene. Additionally, a thermal filtration experiment was also conducted. When the conversion of 3-nitrostyrene reaches 28.9%, the Co@NC-800 catalyst is removed from the mixture using centrifugation, and the residual solution continues to react. As shown in Fig. S6b, the substrate in the reaction solution is not further converted, confirming that the hydrogenation reaction proceeds *via* a heterogeneous process on Co@NC-800.

© Science China Press and Springer-Verlag GmbH Germany, part of Springer Nature 2022

Table 1 Hydrogenation of 3-nitrostyrene using different Co catalysts[a]

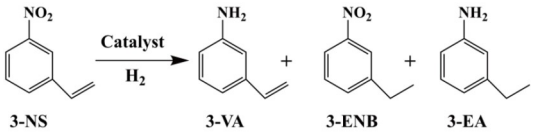

Entry	Catalyst	Conv. (%)	Sel. (%)			TOF[d] (h^{-1})
			3-VA	3-ENB	3-EA	
1	Co@NC-600	5.1	0	33.7	66.3	–
2	Co@NC-700	53.4	98.5	0.9	0.6	4.4
3[b]	Co@NC-800	100	>99	n.d.	n.d.	14.8
4	Co@NC-900	49.7	92.3	2.6	5.1	3.9
5[b,c]	Co@NC-800 (HCl)	100	97.4	0	2.6	–

a) Reaction conditions: 0.5 mmol 3-nitrostyrene, 0.05 g catalyst, 5 mL toluene, 80°C, 3 MPa H_2, 4 h. Internal standard: 1,3,5-trimethylbenzene. b) The reaction time was 2 h. c) Co@NC-800 was refluxed in 1 mol L^{-1} HCl solution at 90°C for 24 h. d) The TOF value was calculated based on the dispersion of Co particles. n.d.: not detected.

Table 2 Results of the chemoselective hydrogenation of various nitroarenes over Co@NC-800[a]

Entry	Substrate	Product	*t* (h)	Yield (%)[b]
1[c]	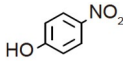	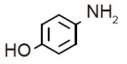	2	99
2[c]	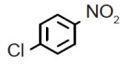	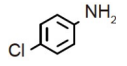	2	99
3	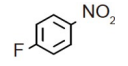	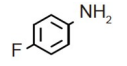	2	99
4[d]	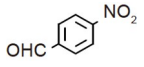	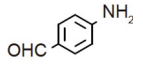	7	99
5	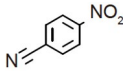	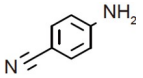	3.5	99
6	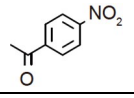	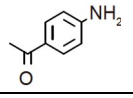	2	99

a) Reaction conditions: 0.5 mmol nitroarene, 0.05 g catalyst, 5 mL toluene, 80°C, 3 MPa H_2; >99% conversion was observed in all cases. b) Determined using GC and GC-MS (internal standard: 1,3,5-trimethylbenzene). c) Solvent: 5 mL ethanol. d) The reaction temperature was 100°C.

The universality of substrates for the Co@NC-800 catalyst was investigated with different substituted nitro compounds. As listed in Table 2, the results show that this catalyst exhibits 99% yield in the chemoselective hydrogenation of various substituted nitroarenes containing electron-donating (–OH), electron-withdrawing (–X), and other reducible groups (such as aldehyde, nitrile, and ketone). These results demonstrate that the Co@NC-800 catalyst can achieve good versatility with high efficiency for the hydrogenation of diverse nitroarenes to the corresponding functional aniline.

To further confirm the encapsulated Co NPs as active centers, a supplement experiment was conducted, where the Co@NC-800 catalyst was refluxed in 1 mol L^{-1} HCl solution at 90°C for 24 h, which can enable the etching of surface-exposed Co species [41]. The resulting catalyst was denoted as Co@NC-800 (HCl). The XRD results in Fig. S7 show that the intensity of the Co diffraction peak does not change after acid treatment. In the performance test, the resultant Co@NC-800(HCl) catalyst still maintains the same catalytic activity as the Co@NC-800 catalyst (Table 1, entry 5). Additionally, the XPS result in Fig. S9 shows almost no presence of residual Zn species on the Co@NC-800 (HCl) catalyst. Thus, the Zn species should not influence the catalytic performance by comparing the experimental results of Co@NC-800(HCl) and Co@NC-800. Moreover, the ICP test results show that the Co content of the Co@NC-800(HCl) catalyst is 19.7%, similar to that of the fresh Co@NC-800 catalyst (20.5%). These results demonstrate the good leaching-resistant ability of the active Co species for the hydrogenation reaction, which can be derived from the encapsulation using the N-doping carbon layer.

Establishment of structure-performance relationship

The above experimental results revealed that the Co@NC-800 catalyst performs better than other pyrolyzed catalysts. To identify the coordination environment and the corresponding chemical state of Co species in Co@NC-X catalysts, X-ray absorption spectroscopy, including XANES and EXAFS, was performed. The standard samples containing Co foil and Co_2O_3 were also characterized as references for a better analysis. As shown in the XANES spectra (Fig. 3a), the Co K-edge of

 © Science China Press and Springer-Verlag GmbH Germany, part of Springer Nature 2022

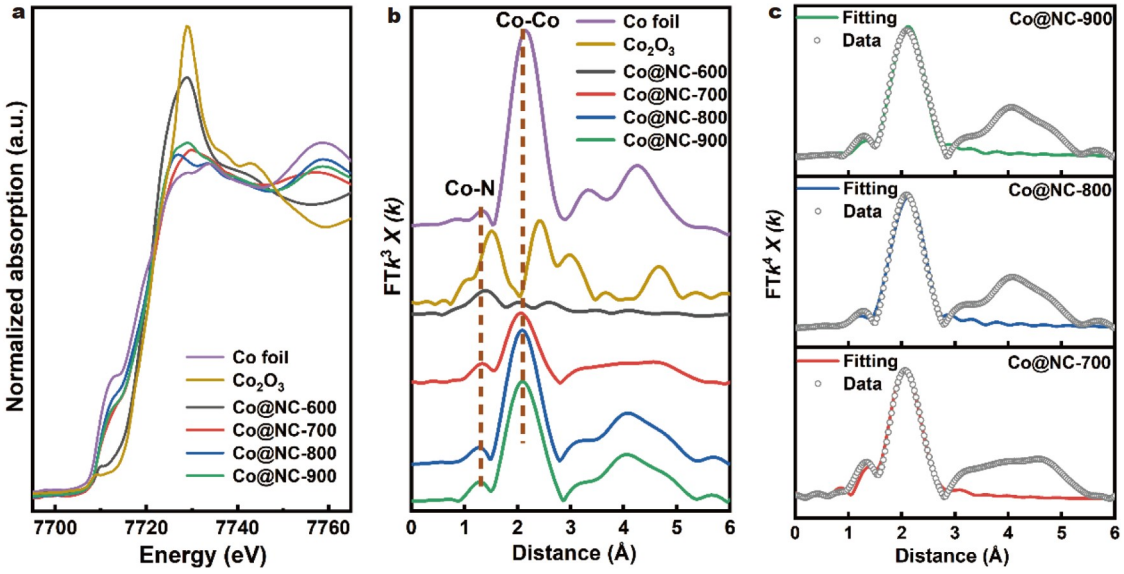

Figure 3 (a) Co-K-edge XANES spectra of different Co@NC-X catalysts with Co_2O_3 and Co foil as references, (b) FT of the Co-K-edge, and (c) EXAFS analysis of different catalysts at *R*-space.

Table 3 The well-fitted EXAFS results of different Co@NC-X catalysts[a]

Sample	Shell	CN	*R* (Å)	σ^2 (10^{-2} Å^2)	ΔE_0 (eV)	*r*-factor (%)
Co Foil	Co–Co	12.0	2.53	–	–	–
Co@NC-700	Co–N	1.3	2.00	0.8	6.6	0.02
	Co–Co	6.0	2.50	0.8	−9.6	
Co@NC-800	Co–N	3.3	2.07	0.8	−3.0	0.02
	Co–Co	9.3	2.51	0.8	−3.0	
Co@NC-900	Co–N	2.1	2.01	0.8	−3.5	0.01
	Co–Co	9.2	2.51	0.8	−3.5	

a) CN is the coordination number for the absorber-backscatterer pair, *R* is the average absorber-backscatterer distance, σ^2 is the Debye-Waller factor, and ΔE_0 is the inner potential correction. The accuracies of the above parameters are estimated as CN, ±20%; *R*, ±10%; σ^2, ± 20%; ΔE_0, ±20%. The data ranges used for data fitting in *k*-space (Δk) and *R*-space (ΔR) are 3.0–10.0 and 1.0–3.0 Å, respectively.

Co@NC-800 catalyst, as well as of Co@NC-700 and Co@NC-900 catalysts, shows the similar white-line intensity compared with the Co foil, indicating that the Co sites exhibit a slightly positive charge on all of these catalysts. In contrast, the Co species in the Co@NC-600 catalyst exhibits an obviously higher valence state, close to Co_2O_3. Combined with the performance test results in Table 1, it is revealed that metallic Co species rather than positive ones are beneficial for the hydrogenation reaction.

The further transformation results to R-space demonstrate that all Co@NC-700, Co@NC-800, and Co@NC-900 show the main peak at 2.1 Å, which is assigned to the Co–Co contribution, as shown in Fig. 3b. Meanwhile, the obvious Co–N species were observed (~1.4 Å) [45,46], indicating that the Co species on these catalysts coexist in the form of Co–Co and Co–N species. Comparatively, Co@NC-600 displays a peak that might be attributed to Co–O coordination due to more positive Co species. Coupled with the performance test results, we mainly focused on comparing Co@NC-700, Co@NC-800, and Co@NC-900 to construct the relationship between Co species and the hydrogenation performances.

Fig. 3c and Table 3 summarize the fitted EXAFS results. It can be seen that the coordination number of Co–Co is 6.0 for the Co@NC-700 catalyst and increases to 9.3 and 9.2 for the Co@NC-800 and Co@NC-900 catalysts, respectively, which corroborate the particle sizes of the corresponding catalysts in the range of 7.5–10 nm (Fig. S4 and Table S1). This demonstrates that the coordination number of Co–Co and the particle size of metal Co do not obviously affect the catalytic performance. As for Co–N species, the Co@NC-800 catalyst has a higher coordination number of 3.3 than Co@NC-700 with 1.3 and Co@NC-900 with 2.1, which is consistent with the trend of the catalytic activity, indicating that the Co–N species can act as the active sites in the hydrogenation of 3-nitrostyrene.

To confirm the importance of Co–N species, XPS measurements were performed to examine the elemental contents and chemical states of Co@NC-X catalysts. As shown in Fig. 4, N 1s XPS spectra are deconvoluted into different N species for various pyrolyzed catalysts. For Co@NC-800, the binding energies exist at 398.7, 400.3, 401.3, and 403.4 eV, which can be assigned to pyridinic N, Co–N, pyrrolic N, and graphitic N [47], respectively. For the Co@NC-600 catalyst, only pyridinic N and pyrrolic N exist. Co–N species can be observed when the pyrolysis temperature reaches 700°C. Interestingly, it is observed in Fig. 4 and Table S3 that the content of Co–N species increases along

 © Science China Press and Springer-Verlag GmbH Germany, part of Springer Nature 2022

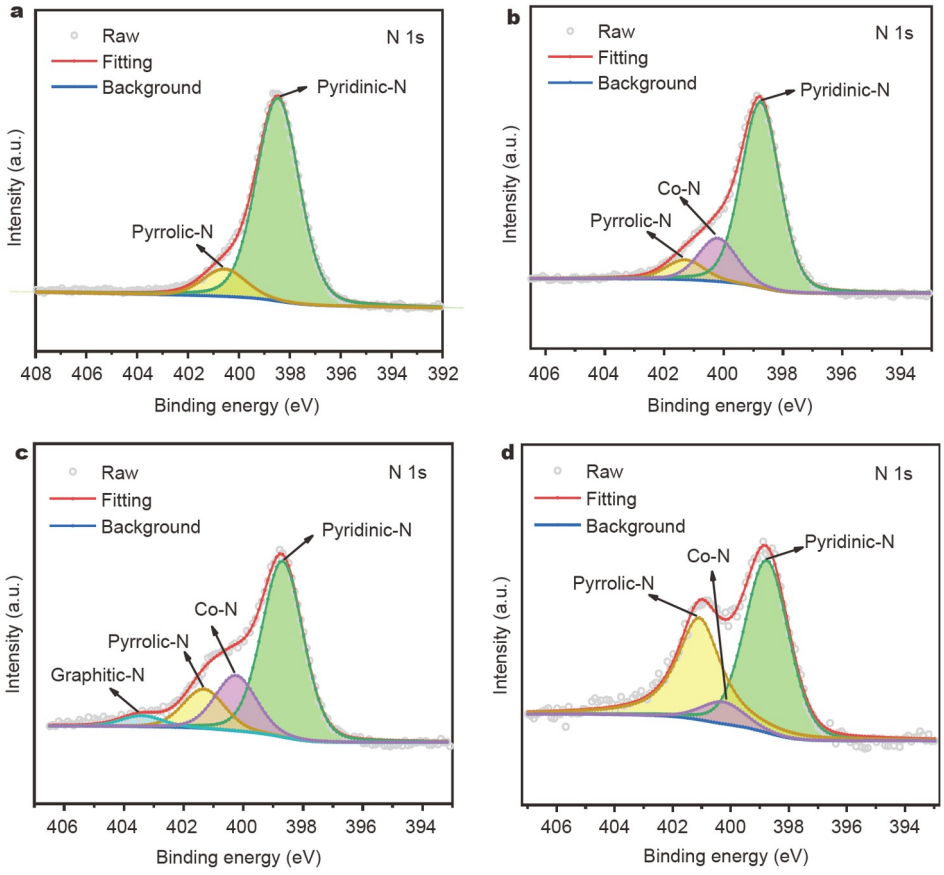

Figure 4 XPS spectra of N 1s region for (a) Co@NC-600, (b) Co@NC-700, (c) Co@NC-800, and (d) Co@NC-900 catalysts.

with the pyrolysis temperature to 800°C but descends at 900°C. Therein, the Co@NC-800 catalyst possesses the largest number of Co–N species. This further verifies that the coordination environment of Co NPs, specifically the Co–N species, can be effectively tuned by altering the pyrolysis temperature. Moreover, it is revealed that the number of Co–N species can determine the hydrogenation performance of 3-nitrostyrene on Co@NC-X catalysts, the trend of which is well consistent with that analyzed using EXAFS characterization.

DISCUSSION

Catalysts containing Co–N species have been extensively studied using pyrolysis strategies with different precursors, such as well-defined cobalt complexes [26,48], a mixture of cobalt salts and N-containing carbon source [44,49], as well as MOFs [29,31,50,51]. Therein, thermal decomposition of MOFs, with high surface area and different metals, has been demonstrated as a facile route to synthesize N-doping porous carbon-supported Co-based materials. However, most of the reported methods require crystalline MOFs as a precursor, which consumes a large amount of solvent in the preparation process and the subsequent washing procedure, resulting in severe environmental issues. This study developed a new and green method to prepare an efficient Co@NC-X catalyst without using any solvent, in which zinc and cobalt salts and 2-MeIM ligand were mixed in the solid state, then dried and pyrolyzed under the optimized condition. This synthesis method can result in the catalytic formulation of Co@NC with a structure of nitrogen-doped graphene shell with encapsulated Co NPs that have strong bonding between N species and Co sites, as suggested in Fig. 2. The resulting Co@NC-800 catalyst exhibits good catalytic performance in the selective hydrogenation of 3-nitrostyrene, yielding ~100% conversion and >99% selectivity to 3-vinylaniline. Meanwhile, the catalyst displays good stability and substrate universality.

Although the materials containing Co–N species have been investigated in the selective hydrogenation of nitroarene, there are still some debates on Co-relevant active sites, such as metal Co particles, graphite-encapsulated metal Co particles, and atomically dispersed Co–N_x species [36,50]. Here, the active sites were absolutely confirmed as Co–N species using the analysis of XAFS, XPS, and experimental results. It was found that the coordination number of Co–Co and particle size of metal Co did not affect the catalytic performance, according to Table 3 and Table S1. In contrast, the valence state of Co species played an important role in the hydrogenation reaction, where slightly positive Co species in the catalysts pyrolyzed at 700, 800, and 900°C showed better catalytic performance than highly positive Co species in the Co@NC-600 catalyst as listed in Table 1. Comparatively, the Co–N species played a critical role in the hydrogenation reaction, of which different pyrolysis temperatures can tune the content of Co–N species. In detail, it can be observed from Fig. 5 that an obvious relationship with a volcano-like profile between hydrogenation performance and Co–N coordination number and Co–N amount can be established, where the Co@NC-800 catalyst with rich Co–N species and higher coordination number exhibited the best catalytic

 © Science China Press and Springer-Verlag GmbH Germany, part of Springer Nature 2022

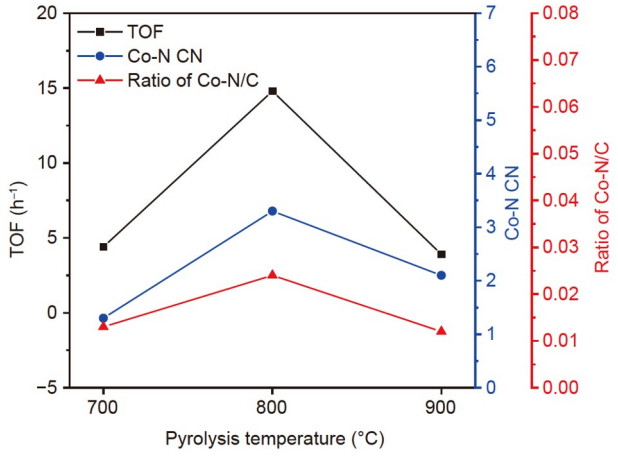

Figure 5 The relationships between hydrogenation activity, Co–N content, and Co–N coordination number, and the pyrolysis temperatures for Co@NC-X catalysts.

performance. These results indicate that the Co–N content is positively related to the hydrogenation performance, unequivocally confirming the Co–N species as the active sites.

On the Co@NC-800 catalyst, there is a strong interaction between the active sites and the substrate, where metallic Co particles are in close contact with N-doped carbon, and the electron transfer exists at the interface of Co and N-doped carbon [52–54]. This can result in the redistribution of electrons and formation of an electron-rich region in the N-doped carbon shell due to the Mott-Schottky base effect [38,54,55]. For 3-nitrostyrene, the $-NO_2$ group of this reactant is electron-deficient, which is facile to be attracted by the electron-rich carbon substrate [31]. Thus, the Co–N centers of the Co@NC-800 catalyst can facilitate the adsorption of 3-nitrostyrene. Additionally, the encapsulated Co particles using N-doped carbon shells are favorable for improved selectivity. Due to this, the exposed Co NPs can lead to the coadsorption of two or more functional groups for decreased selectivity [38]. Therefore, the encapsulated structure of Co@NC-800, which contains more Co–N active species than other Co@NC-X catalysts, can simultaneously enhance the activity and selectivity in the hydrogenation of nitroarenes.

Additionally, Co@NC-800 can also adsorb H_2 reactants according to the H_2-TPD result (Fig. S10). The metallic Co NPs and doped nitrogen species can facilitate the activation of H_2 in the dissociated form [53,56,57]. This phenomenon was further analyzed by investigating the kinetic parameters of H_2 pressure for different catalysts. As shown in Fig. S11, the H_2 reaction orders over the Co@NC-700, Co@NC-800, and Co@NC-900 catalysts were calculated to be 1.28, 0.78, and 1.71, respectively. The lower the reaction order, the weaker the dependence of the catalytic performance on the adsorption of reactants, that is, the higher the coverage of the reactant on the active sites [44,58]. Thus, the lowest value of H_2 reaction order on the Co@NC-800 catalyst suggested the most feasible activation of H_2, which originated from the abundant Co–N species for its dissociation [44,59]. This property facilitated the further hydrogenation of 3-nitrostyrene with high activity and selectivity on Co@NC-800.

CONCLUSIONS

In summary, a green and facile method was explored to prepare a nitrogen-doped graphene shell-encapsulated Co catalyst without employing any solvent. The prepared Co@NC-800 catalyst exhibits excellent catalytic performance in the selective hydrogenation of 3-nitrostyrene, achieving 100% conversion and >99% selectivity for 3-vinylaniline under relatively mild conditions (80°C and 3 MPa). Moreover, it exhibits good versatility to other substrates with a reducible group and excellent reusability. The superior performance can be attributed to the role of the unique encapsulated structure and the active Co–N species, which can be tuned by changing the pyrolysis temperature. The proposed strategy here provides a novel way to synthesize Co-based catalysts in an environment-friendly approach.

Received 10 March 2022; accepted 7 May 2022; published online 28 July 2022

1 Han A, Zhang J, Sun W, *et al.* Isolating contiguous Pt atoms and forming Pt-Zn intermetallic nanoparticles to regulate selectivity in 4-nitrophenylacetylene hydrogenation. Nat Commun, 2019, 10: 3787
2 Huang L, Lv Y, Wu S, *et al.* Activated carbon supported bimetallic catalysts with combined catalytic effects for aromatic nitro compounds hydrogenation under mild conditions. Appl Catal A-Gen, 2019, 577: 76–85
3 Beswick O, Parastaev A, Yuranov I, *et al.* Highly dispersed cobalt oxides nanoparticles on activated carbon fibres as efficient structured catalysts for the transfer hydrogenation of *m*-nitrostyrene. Catal Today, 2017, 279: 29–35
4 Camacho-Bunquin J, Ferrandon M, Sohn H, *et al.* Chemoselective hydrogenation with supported organoplatinum(IV) catalyst on Zn(II)-modified silica. J Am Chem Soc, 2018, 140: 3940–3951
5 Formenti D, Ferretti F, Scharnagl FK, *et al.* Reduction of nitro compounds using 3d-non-noble metal catalysts. Chem Rev, 2019, 119: 2611–2680
6 Macino M, Barnes AJ, Althahban SM, *et al.* Tuning of catalytic sites in Pt/TiO_2 catalysts for the chemoselective hydrogenation of 3-nitrostyrene. Nat Catal, 2019, 2: 873–881
7 Nandi D, Siwal S, Choudhary M, *et al.* Carbon nitride supported palladium nanoparticles: An active system for the reduction of aromatic nitro-compounds. Appl Catal A-Gen, 2016, 523: 31–38
8 Tamura M, Yuasa N, Nakagawa Y, *et al.* Selective hydrogenation of nitroarenes to aminoarenes using a MoO_x-modified Ru/SiO_2 catalyst under mild conditions. Chem Commun, 2017, 53: 3377–3380
9 Chen G, Xu C, Huang X, *et al.* Interfacial electronic effects control the reaction selectivity of platinum catalysts. Nat Mater, 2016, 15: 564–569
10 Chen LW, Tong L, Nan H, *et al.* Sub-2 nm Ir nanoclusters immobilized on mesoporous nitrogen-doped carbons as efficient catalysts for selective hydrogenation. ACS Appl Nano Mater, 2019, 2: 6546–6553
11 Fu H, Zhang L, Wang Y, *et al.* Thermally reduced gold nanocatalysts prepared by the carbonization of ordered mesoporous carbon as a heterogeneous catalyst for the selective reduction of aromatic nitro compounds. J Catal, 2016, 344: 313–324
12 Guo M, Li H, Ren Y, *et al.* Improving catalytic hydrogenation performance of Pd nanoparticles by electronic modulation using phosphine ligands. ACS Catal, 2018, 8: 6476–6485
13 Leng F, Gerber IC, Lecante P, *et al.* Controlled and chemoselective hydrogenation of nitrobenzene over $Ru@C_{60}$ catalysts. ACS Catal, 2016, 6: 6018–6024
14 Lin L, Yao S, Gao R, *et al.* A highly CO-tolerant atomically dispersed Pt catalyst for chemoselective hydrogenation. Nat Nanotechnol, 2019, 14: 354–361
15 Mitsudome T, Kaneda K. Gold nanoparticle catalysts for selective hydrogenations. Green Chem, 2013, 15: 2636–2654
16 Tomkins P, Gebauer-Henke E, Leitner W, *et al.* Concurrent hydrogenation of aromatic and nitro groups over carbon-supported ruthenium catalysts. ACS Catal, 2014, 5: 203–209
17 Pan H, Peng Y, Lu X, *et al.* Well-constructed Ni@CN material derived from di-ligands Ni-MOF to catalyze mild hydrogenation of nitroarenes.

 © Science China Press and Springer-Verlag GmbH Germany, part of Springer Nature 2022

Mol Catal, 2020, 485: 110838
18 Wei Z, Mao S, Sun F, *et al.* The synergic effects at the molecular level in CoS_2 for selective hydrogenation of nitroarenes. Green Chem, 2018, 20: 671–679
19 Cui X, Liang K, Tian M, *et al.* Cobalt nanoparticles supported on N-doped mesoporous carbon as a highly efficient catalyst for the synthesis of aromatic amines. J Colloid Interface Sci, 2017, 501: 231–240
20 Fang H, Wen M, Chen H, *et al.* Graphene stabilized ultra-small CuNi nanocomposite with high activity and recyclability toward catalysing the reduction of aromatic nitro-compounds. Nanoscale, 2016, 8: 536–542
21 Jagadeesh RV, Stemmler T, Surkus AE, *et al.* Cobalt-based nanocatalysts for green oxidation and hydrogenation processes. Nat Protoc, 2015, 10: 916–926
22 Lu X, He J, Jing R, *et al.* Microwave-activated Ni/carbon catalysts for highly selective hydrogenation of nitrobenzene to cyclohexylamine. Sci Rep, 2017, 7: 2676
23 Ma Y, Lang Z, Du J, *et al.* A switchable-selectivity multiple-interface Ni-WC hybrid catalyst for efficient nitroarene reduction. J Catal, 2019, 377: 174–182
24 Ma Z, Liu H, Yue M. Magnetically recyclable Sm_2Co_{17}/Cu catalyst to chemoselectively reduce the 3-nitrostyrene into 3-vinylaniline under room temperature. Nano Res, 2019, 12: 3085–3088
25 Sorribes I, Liu L, Corma A. Nanolayered Co-Mo-S catalysts for the chemoselective hydrogenation of nitroarenes. ACS Catal, 2017, 7: 2698–2708
26 Westerhaus FA, Jagadeesh RV, Wienhöfer G, *et al.* Heterogenized cobalt oxide catalysts for nitroarene reduction by pyrolysis of molecularly defined complexes. Nat Chem, 2013, 5: 537–543
27 Goswami A, Kadam RG, Tuček J, *et al.* Fe(0)-embedded thermally reduced graphene oxide as efficient nanocatalyst for reduction of nitro compounds to amines. Chem Eng J, 2020, 382: 122469
28 Gao R, Guo H, Wang B, *et al.* Co based N, S co-doped carbon hybrids for catalytic hydrogenation: Role of cobalt salt and doped S. Appl Catal A-Gen, 2019, 579: 99–105
29 Lan X, Ali B, Wang Y, *et al.* Hollow and yolk-shell Co-N-C@SiO_2 nanoreactors: Controllable synthesis with high selectivity and activity for nitroarene hydrogenation. ACS Appl Mater Interfaces, 2020, 12: 3624–3630
30 Sun X, Olivos-Suarez AI, Oar-Arteta L, *et al.* Metal-organic framework mediated cobalt/nitrogen-doped carbon hybrids as efficient and chemoselective catalysts for the hydrogenation of nitroarenes. ChemCatChem, 2017, 9: 1854–1862
31 Wang X, Li Y. Chemoselective hydrogenation of functionalized nitroarenes using MOF-derived co-based catalysts. J Mol Catal A-Chem, 2016, 420: 56–65
32 Chen FF, Chen J, Feng YN, *et al.* Controlling metallic Co^0 in ZIF-67-derived N-C/Co composite catalysts for efficient photocatalytic CO_2 reduction. Sci China Mater, 2022, 65: 413–421
33 Zhang J, Chen Y, Liu Y, *et al.* Self-catalyzed growth of Zn/Co-N-C carbon nanotubes derived from metal-organic frameworks as efficient oxygen reduction catalysts for Zn-air battery. Sci China Mater, 2022, 65: 653–662
34 Qi Z, Pei Y, Goh TW, *et al.* Conversion of confined metal@ZIF-8 structures to intermetallic nanoparticles supported on nitrogen-doped carbon for electrocatalysis. Nano Res, 2018, 11: 3469–3479
35 Wang X, Chen W, Zhang L, *et al.* Uncoordinated amine groups of metal-organic frameworks to anchor single Ru sites as chemoselective catalysts toward the hydrogenation of quinoline. J Am Chem Soc, 2017, 139: 9419–9422
36 Li M, Chen S, Jiang Q, *et al.* Origin of the activity of Co-N-C catalysts for chemoselective hydrogenation of nitroarenes. ACS Catal, 2021, 11: 3026–3039
37 Peera SG, Balamurugan J, Kim NH, *et al.* Sustainable synthesis of Co@NC core shell nanostructures from metal organic frameworks *via* mechanochemical coordination self-assembly: An efficient electrocatalyst for oxygen reduction reaction. Small, 2018, 14: 1800441
38 Chen S, Ling LL, Jiang SF, *et al.* Selective hydrogenation of nitroarenes under mild conditions by the optimization of active sites in a well defined Co@NC catalyst. Green Chem, 2020, 22: 5730–5741
39 Wei H, Liu X, Wang A, *et al.* FeO_x-supported platinum single-atom and pseudo-single-atom catalysts for chemoselective hydrogenation of functionalized nitroarenes. Nat Commun, 2014, 5: 5634
40 Bergeret G, Gallezot P. Particle size and dispersion measurements. Handbook of Heretogeneous Catalysis, 2008, 2: 738–765
41 Liu L, Concepción P, Corma A. Non-noble metal catalysts for hydrogenation: A facile method for preparing Co nanoparticles covered with thin layered carbon. J Catal, 2016, 340: 1–9
42 Schwob T, Kempe R. A reusable Co catalyst for the selective hydrogenation of functionalized nitroarenes and the direct synthesis of imines and benzimidazoles from nitroarenes and aldehydes. Angew Chem Int Ed, 2016, 55: 15175–15179
43 Liu L, Gao F, Concepción P, *et al.* A new strategy to transform mono and bimetallic non-noble metal nanoparticles into highly active and chemoselective hydrogenation catalysts. J Catal, 2017, 350: 218–225
44 Wei Z, Wang J, Mao S, *et al.* *In situ*-generated Co^0-Co_3O_4/N-doped carbon nanotubes hybrids as efficient and chemoselective catalysts for hydrogenation of nitroarenes. ACS Catal, 2015, 5: 4783–4789
45 Sun T, Zhao S, Chen W, *et al.* Single-atomic cobalt sites embedded in hierarchically ordered porous nitrogen-doped carbon as a superior bifunctional electrocatalyst. Proc Natl Acad Sci USA, 2018, 115: 12692–12697
46 Yu P, Wang L, Sun F, *et al.* Co nanoislands rooted on Co-N-C nanosheets as efficient oxygen electrocatalyst for Zn-air batteries. Adv Mater, 2019, 31: 1901666
47 Zhou D, Zhang L, Liu X, *et al.* Tuning the coordination environment of single-atom catalyst M-N-C towards selective hydrogenation of functionalized nitroarenes. Nano Res, 2022, 15: 519–527
48 Zhang L, Wang A, Wang W, *et al.* Co-N-C catalyst for C–C coupling reactions: On the catalytic performance and active sites. ACS Catal, 2015, 5: 6563–6572
49 Li H, Cao C, Liu J, *et al.* Cobalt single atoms anchored on N-doped ultrathin carbon nanosheets for selective transfer hydrogenation of nitroarenes. Sci China Mater, 2019, 62: 1306–1314
50 Jagadeesh RV, Murugesan K, Alshammari AS, *et al.* MOF-derived cobalt nanoparticles catalyze a general synthesis of amines. Science, 2017, 358: 326–332
51 Yang S, Peng L, Oveisi E, *et al.* MOF-derived cobalt phosphide/carbon nanocubes for selective hydrogenation of nitroarenes to anilines. Chem Eur J, 2018, 24: 4234–4238
52 Chen T, Guo S, Yang J, *et al.* Nitrogen-doped carbon activated *in situ* by embedded nickel through the Mott-Schottky effect for the oxygen reduction reaction. ChemPhysChem, 2017, 18: 3454–3461
53 Deng D, Yu L, Chen X, *et al.* Iron encapsulated within pod-like carbon nanotubes for oxygen reduction reaction. Angew Chem Int Ed, 2013, 52: 371–375
54 Wang J, Wei Q, Ma Q, *et al.* Constructing Co@N-doped graphene shell catalyst *via* Mott-Schottky effect for selective hydrogenation of 5-hydroxylmethylfurfural. Appl Catal B-Environ, 2020, 263: 118339
55 Xue ZH, Han JT, Feng WJ, *et al.* Tuning the adsorption energy of methanol molecules along Ni-N-doped carbon phase boundaries by the Mott-Schottky effect for gas-phase methanol dehydrogenation. Angew Chem Int Ed, 2018, 57: 2697–2701
56 Fu T, Wang M, Cai W, *et al.* Acid-resistant catalysis without use of noble metals: Carbon nitride with underlying nickel. ACS Catal, 2014, 4: 2536–2543
57 Zhang L, Zhou M, Wang A, *et al.* Selective hydrogenation over supported metal catalysts: From nanoparticles to single atoms. Chem Rev, 2020, 120: 683–733
58 Wang L, Zhu C, Xu M, *et al.* Boosting activity and stability of metal single-atom catalysts *via* regulation of coordination number and local composition. J Am Chem Soc, 2021, 143: 18854–18858
59 Xiong W, Zhou S, Wang L, *et al.* ZIF-derived Co-based catalysts for efficient hydrogenation of aromatic compounds: The study of the Co–N_x active sites. Ind Eng Chem Res, 2020, 59: 22473–22484

Acknowledgements This work was supported by the National Natural Science Foundation of China (21808193, 21878283, 22022814, and

 © Science China Press and Springer-Verlag GmbH Germany, part of Springer Nature 2022

22002118), China Postdoctoral Science Foundation (2020TQ0245), the Science and Technology Innovation Development Plan of Yantai (2021XDHZ069), the Youth Innovation Promotion Association CAS (Y2021057), Dalian Science Foundation for Distinguished Young Scholars (2021RJ10), and Taishan Scholars Program of Shandong province (tsqn202103051).

Author contributions Wei H, Song H and Ren Y participated in the design of this study, conducted the experiments, performed data analysis and drafted the manuscript. Yan X and Fang G conducted the experiments. Wang W, Ren W and Zhu M provided assistance for the data acquisition and analysis. Lin J proposed the idea, supervised the research and revised the manuscript. All authors read and approved the content of the manuscript.

Conflict of interest The authors declare that they have no conflict of interest.

Supplementary information Supporting data are available in the online version of the paper.

Haisheng Wei received his PhD degree from Dalian Institute of Chemical Physics (DICP), Chinese Academy of Sciences (CAS) under the supervision of Prof. Aiqin Wang and Prof. Tao Zhang in 2015. His research interests focus on the design, synthesis and characterization of highly dispersed supported metal catalysts for the synthesis of fine chemicals.

Huaxing Song is currently a master student at the College of Chemistry and Chemical Engineering, Yantai University. His research interest focuses on the development of MOFs-derived materials and their corresponding performances in selective hydrogenation reactions.

Yujing Ren is currently an associate professor at the School of Life Sciences, Northwestern Polytechnical University (NWPU). He received his PhD degree from DICP, CAS under the supervision of Prof. Dangsheng Su, Prof. Aiqin Wang and Prof. Tao Zhang in 2020, and then joined the NWPU. His research interests include single-atom catalysis, selective hydrogenation/hydrogenolysis reactions and nanozyme.

Jian Lin received his PhD degree from the DICP, CAS in 2011. He is now a professor at the DICP. His research interests include controlled syntheses and characterizations of highly dispersed metal catalysts, and their applications in heterogeneous oxidation and hydrogenation catalysis.

无溶剂合成以Co–N物种为活性位点的Co@NC催化剂用于芳香硝基化合物选择加氢

魏海生[1†], 宋华兴[1†], 任煜京[3†], 颜晓瑞[1], 方葛钱[2], 王文华[1], 任万忠[1], 朱明远[1], 林坚[2*]

摘要 金属有机骨架(MOFs)衍生的Co基催化剂用于芳香硝基化合物选择加氢引起了广泛的关注, 但催化剂合成过程中使用大量溶剂, 且对催化剂中活性中心的认识存在争议. 本文开发了一种固相合成策略, 在不使用任何溶剂的情况下获得MOF前体材料, 经发泡和热解处理获得Co@NC催化剂. 研究发现, 800°C热解所得的催化剂中Co纳米颗粒被氮掺杂石墨烯壳层包裹, 在3-硝基苯乙烯的加氢过程中表现出~100%的转化率, 3-乙烯基苯胺的选择性大于99%, 同时, 该催化剂具有良好的循环稳定性和底物普适性. 表征和实验结果证明该催化剂中Co–N物种为活性中心, 其含量可通过热解温度进行调变, 且催化性能与Co–N物种的含量存在正相关关系. 本工作为设计用于选择加氢反应的高效Co基催化剂提供了一种新的绿色合成策略.

 © Science China Press and Springer-Verlag GmbH Germany, part of Springer Nature 2022